The International Journal of Cardiovascular Imaging (2019) 35:1365–1377
https://doi.org/10.1007/s10554-019-01562-4

REVIEW PAPER

Role of imaging in diagnosis and management of left ventricular assist device complications

Xin Li[1] · Victor Kondray[1] · Sidhartha Tavri[1] · Arjang Ruhparwar[2] · Samuel Azeze[1] · Aritra Dey[1] · Sasan Partovi[3] · Fabian Rengier[4]

Received: 28 December 2018 / Accepted: 11 February 2019 / Published online: 4 March 2019

Abstract

Heart failure is a clinical condition that is associated with significant morbidity and mortality. With the advent of left ventricular assist device (LVAD), an increasing number of patients have received an artificial heart both as a bridge-to-therapy and as a destination therapy. Clinical trials have shown clear survival benefits of LVAD implantation. However, the increased survival benefits and improved quality of life come at the expense of an increased complication rate. Common complications include perioperative bleeding, infection, device thrombosis, gastrointestinal bleeding, right heart failure, and aortic hemodynamic changes. The LVAD-associated complications have unique pathophysiology. Multiple imaging modalities can be employed to investigate the complications, including computed tomography (CT), positron emission tomography-computed tomography (PET-CT), catheter angiography and echocardiography. Imaging studies not only help ascertain diagnosis and evaluate the severity of disease, but also help direct relevant clinical management and predict prognosis. In this article, we aim to review the common LVAD complications, present the associated imaging features and discuss the role of imaging in their management.

Keywords LVAD · Radiology · Complication · Imaging features

Introduction

Heart failure (HF) is a complex medical condition that affects approximately 6 million people in the United States. The disease is characterized by a chronic and progressive reduction of cardiac output unable to meet physiological demands [1]. HF bears a high morbidity and mortality rate [2]. Most importantly, patients with advanced HF have a mortality rate exceeding 50% in 1 year [3].

✉ Sasan Partovi
sxp509@case.edu

[1] Department of Radiology, Section of Interventional Radiology, University Hospitals Cleveland Medical Center, Cleveland, OH, USA

[2] Department of Cardiac Surgery, University Hospital Heidelberg, Heidelberg, Germany

[3] Department of Radiology, Section of Interventional Radiology, Cleveland Clinic Foundation, Cleveland, OH, USA

[4] Department of Diagnostic and Interventional Radiology, University Hospital Heidelberg, Heidelberg, Germany

Although medical management has achieved marked advancement in reducing the overall mortality [4], a small percentage of the patients progress to advanced HF. Orthotopic heart transplantation remains the preferred management for this patient population. However only 2200 patients undergo transplantation each year, representing a small fraction of AHA stage D HF patients [5].

For those who are ineligible for heart transplantation or with no suitable donor, left ventricular assist device (LVAD) has become an attractive option both as a bridge-to-transplant (BTT) and as a destination therapy (DT). LVAD augments the innate cardiac pumping function by creating an artificial blood flow conduit from the left ventricle to either the ascending or descending aorta, thereby supplying the systemic circulation and maintaining proper tissue perfusion. In the United States more than 2500 LVAD implants are placed per year and the number of LVAD device implantations is increasing steadily [6]. LVAD support has greatly reduced the short-term mortality, with 1 and 2 year survival rates of 81% and 72%, respectively [7]. In comparison to the medically managed patients, there was a 48% reduction in all-cause mortality in the LVAD patient population

[3]. However, LVAD is associated with significant numbers of post-implantation adverse events. Bleeding, infection, thrombosis, embolism, hemodynamic alterations, and device malfunction are among the most common complications. In general, major adverse events can be categorized into those that are related to the surgical procedure, innate device properties and associated management, and hemodynamic changes.

In this article, we aim to present the common post-implantation LVAD complications and demonstrate the value of imaging for the diagnosis and management of LVAD complications.

Evolution of LVAD devices

LVAD was first conceptualized in 1964 as an experimental heart replacement therapy under an NIH directed artificial heart initiative [8, 9]. Since then the field has advanced rapidly. The first generation LVADs attempted to mimic the native heart's pulsatile nature. The Randomized Evaluation of Mechanical Assistance for the Treatment of Congestive HF (REMATCH) trail showed 1 and 2 year survival rates of 52% and 23% in the treatment group versus 25% and 8% in the medically managed group [3]. However, it was discovered that the original design had significant issues, perhaps related to its large size and number of moving components [3]. The probability of device failure could reach 72.9% at 2 years [10]. Therefore, the second generation LVADs were developed with a simplified design. It is characterized by its continuous-flow pumping function, thereby allowing size reduction and design simplification. The reliability of the second generation LVAD greatly improved compared to their counterparts in the first generation LVAD. Slaughter et al. reported that only 10% of the continuous-flow LVADs were repaired or replaced in comparison to 36% of the pulsatile-flow LVAD systems. More importantly, the complication-free survival rate was 64% in the second generation LVAD group versus 11% in the HeartMate XVE group [11]. The third generation LVAD, represented by HeartMate 3 (Thoratec Corporation, Pleasanton, CA), uses a centrifugal design [12].

In the early days of LVAD implantation, perioperative mortality rate was as high as 29% [13]. With the advancement of minimally invasive techniques, such as mini-thoracotomy and hemisternotomy, 30 days postoperative mortality has been decreased to as low as 1% in one study [14].

General imaging appearance

Several imaging modalities can be employed to evaluate LVAD and its complications. Echocardiography is often the first-line modality as it is highly portable and cost-effective. However, it is limited by its dependence on user experience and often poor acoustic windows.

Computed tomography (CT) is a robust technique, less observer dependent, widely available and capable of imaging a wide variety of clinical problems. Its disadvantages include the use of radiation, the higher cost compared to echocardiography, and the need for iodinated contrast material for CT angiography which can be contraindicated in patients with severe renal impairment. Besides, LVADs sometimes cause severe beam hardening artifacts limiting the visualization of immediately surrounding structures. The preferred protocol is prospective ECG-gated sequence in arterial phase. In comparison, retrospectively gated scan has a higher radiation exposure but can evaluate cardiac and valvular function depending on the degree of beam hardening artefacts. A typical CT angiography is performed using automated tube voltage and tube current selection and bolus tracking technique. For tracking of the contrast bolus, a region of interest is typically placed in the ascending aorta, and the acquisition is initiated after reaching a threshold of e.g. 150 Hounsfield Units with a 5 s delay. Robust image quality can usually be achieved with 90 ml of iodinated contrast material injected into an antecubital vein at 4 ml/s followed by a saline flush of 30 ml at the same injection rate.

Lastly, magnetic resonance imaging (MRI) is absolutely contraindicated in LVAD patient population as it is not compatible with the devices.

On CT imaging the inflow cannula or pump housing is seen positioned in the apex of the left ventricle with the outflow cannula in the ascending or descending aorta. There should be no thrombus, gas or fluid collection in or around the device. At the normal operating speed of second and third generation LVADs, the aortic valve should remain closed throughout the cardiac cycle. During frequent follow-ups, special attention should be paid to the valvular functions with either retrospectively ECG-gated CT angiography or echocardiography as aortic insufficiency or mitral stenosis can lead to deterioration of the pump function (Figs. 1, 2).

The driveline connects the pump to the external controller and power source. The driveline is typically implanted through the subcutaneous tissue of the abdominal wall. It is important to consider imaging the driveline in its entirety during CT protocoling, as typical chest CT only includes the upper abdomen. An abdominal CT may be included to image the exit site of the driveline.

Perioperative bleeding

Bleeding is a common complication during the early perioperative period. In the REMATCH trial, 46% of the patients experienced major bleeding episodes. Bleeding is typically at the anastomosis between the native heart and the conduits,

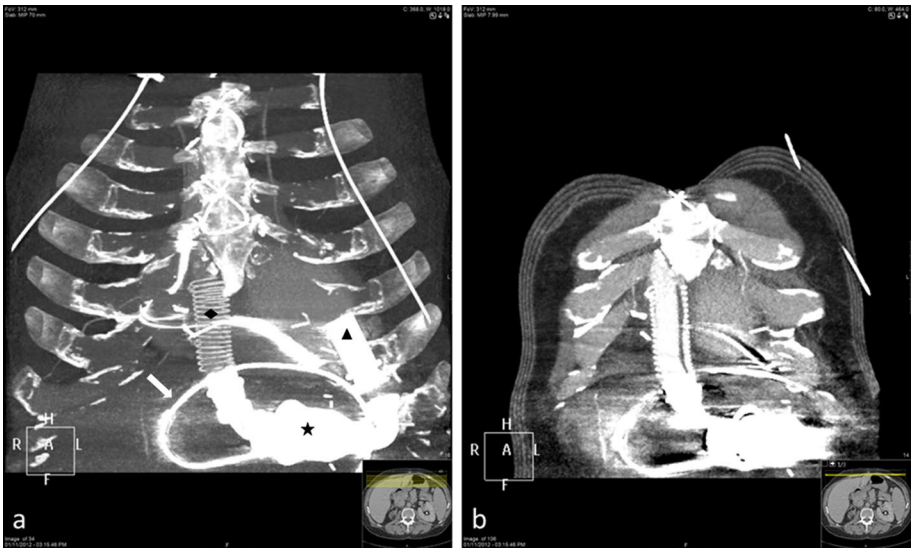

Fig. 1 Normal alignment of LVAD. **a, b** Thick- (**a**) and thin-sliced (**b**) maximum intensity projection images in coronal orientation. Notice the inflow cannula situated in the apex of the heart. Dacron outflow tract situated in the ascending aorta. Notice the artifacts from both the device and driveline. There is also no noticeable thrombus, fluid or gas collection in and near the anastomosis sites. Black triangle marks the inflow cannula. Black star represents the body of LVAD. Black diamond is the outflow cannula and the white arrow points at the driveline

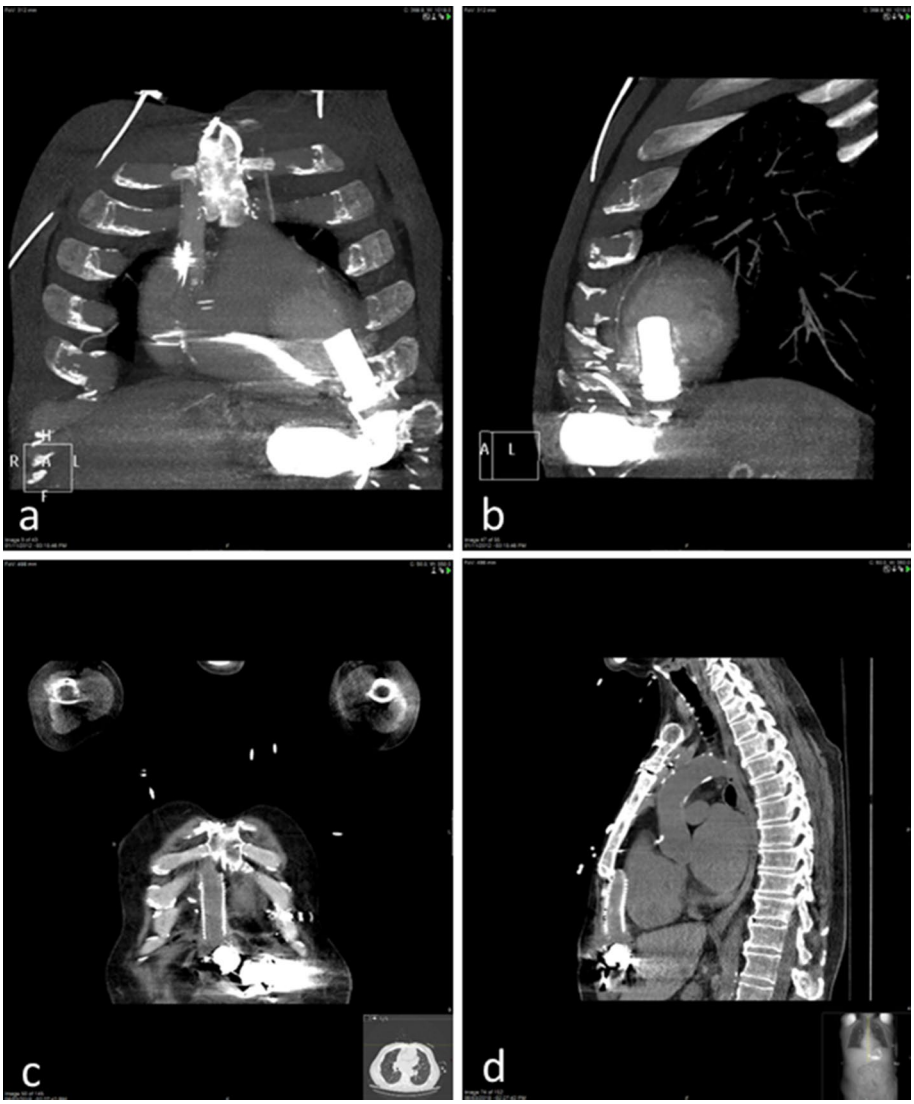

Fig. 2 62 year-old male with a history of non-ischemic cardiomyopathy received LVAD placement as a BTT. 7 years after the initial placement, patient experienced pump malfunction with increased power spikes. **a, b** MIP image of the LVAD at 1 year post-operation, demonstrating angulated inflow cannula in the apex of the left ventricle. Notice it is not obstructed, although cardiac-cycle related obstruction can only be seen on ECG-gated CT. **c, d** Coronal and sagittal images show the apparent discontinuity between the device body and the outflow cannula, correlating with the device malfunction

and blood commonly pools in the mediastinum and the pericardial space [15].

Bleeding can be visualized on CT imaging as a hyperdense hemorrhagic collection and possibly an extravasation of contrast in cases of active bleeding. The attenuation of the hemorrhagic process will gradually decrease over time, as blood products continue to break down. Pericardial tamponade is another immediate postoperative complication, which can be depicted on CT [16, 17] (Figs. 3, 4).

Infection

Device infection is a common late complication. Although the size of LVAD has decreased over time, most contemporary designs retain a driveline that traverses the abdominal wall, breaks through the skin barrier, and connects to an external battery package [18]. In addition, LVADs have multiple blood contacting surfaces by the nature of its design. Fibrin deposition on the surface of the device and cannulae provides a nidus for bacterial colonization. Further, the driveline cannot be completely immobilized, and this has led to repetitive trauma to the exit site, which creates an opening for bacterial invasion. Indeed, the driveline is frequently implicated as the source of infection. Studies have shown that driveline infection rate ranged between 12 and 23% [19–22]. Such infections increase delayed mortality. In the continuous-flow era, sepsis is associated with a significant increase in mortality for 42 patients (mortality rates of 61.9% vs. 18% at 2 years in septic and non-septic patients, respectively) [23].

On CT imaging, infection may present with a gas or fluid-containing pocket around the driveline or the device. Other CT imaging findings consistent with increased inflammation and/or infectious process include rim-enhancing fluid pockets and soft-tissue stranding. Fluorine 18-fluorodeoxyglucose positron emission tomography

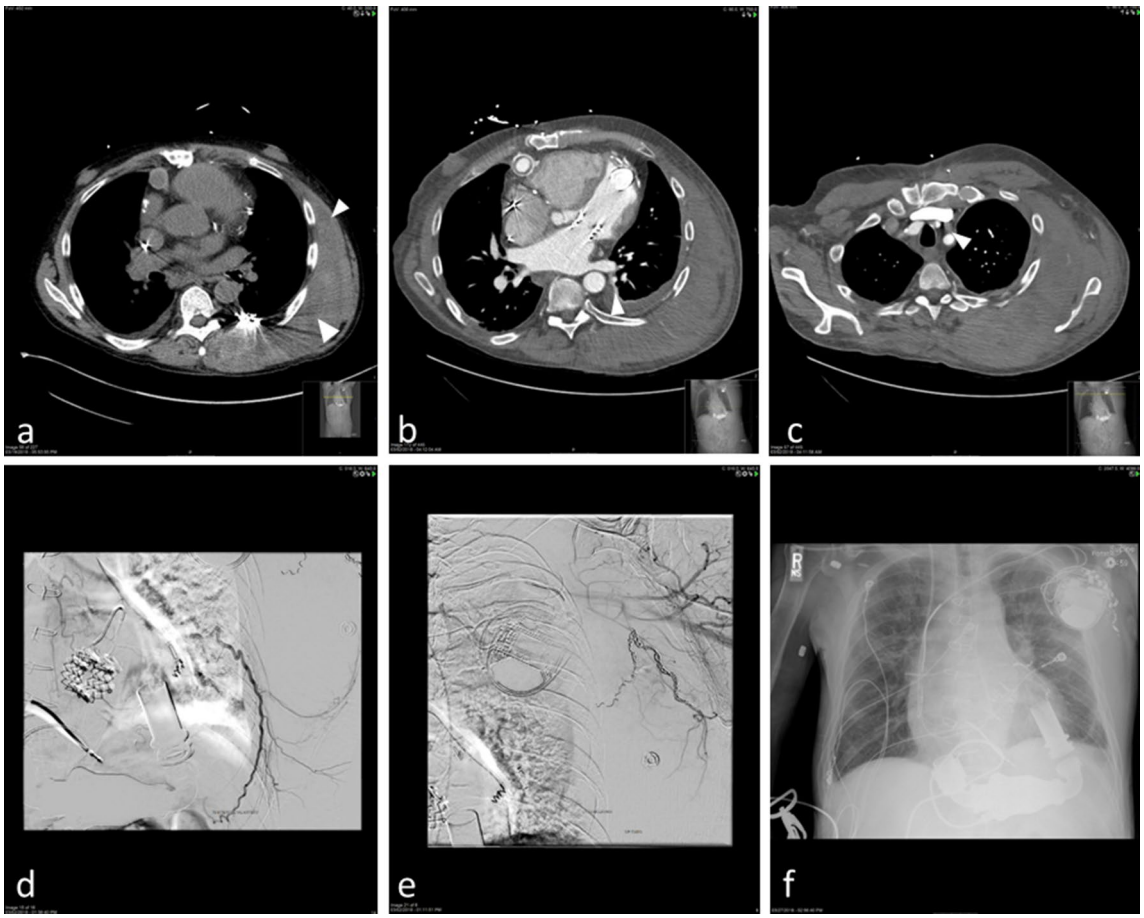

Fig. 3 67 year-old male patient with a history of ischemic cardiomyopathy status post six stents placement. He received LVAD placement as a DT. He later presented with fatigue and chest wall hematoma. **a** Transverse images show significant subcutaneous soft tissue density, correlating with the chest wall hematoma (arrowheads). **b, c** Transverse CT angiography images showing bleeding from left T9 intercostal artery, and lateral thoracodorsal branch of L subclavian, respectively (arrowheads), **d** angiography during embolization procedure again showing the feeder thoracodorsal artery. **e** Post-embolization fluoroscopy image of the same vessel. Notice the placement of coil within the vessel lumen. **f** Chest X-ray shows the LVAD alignment

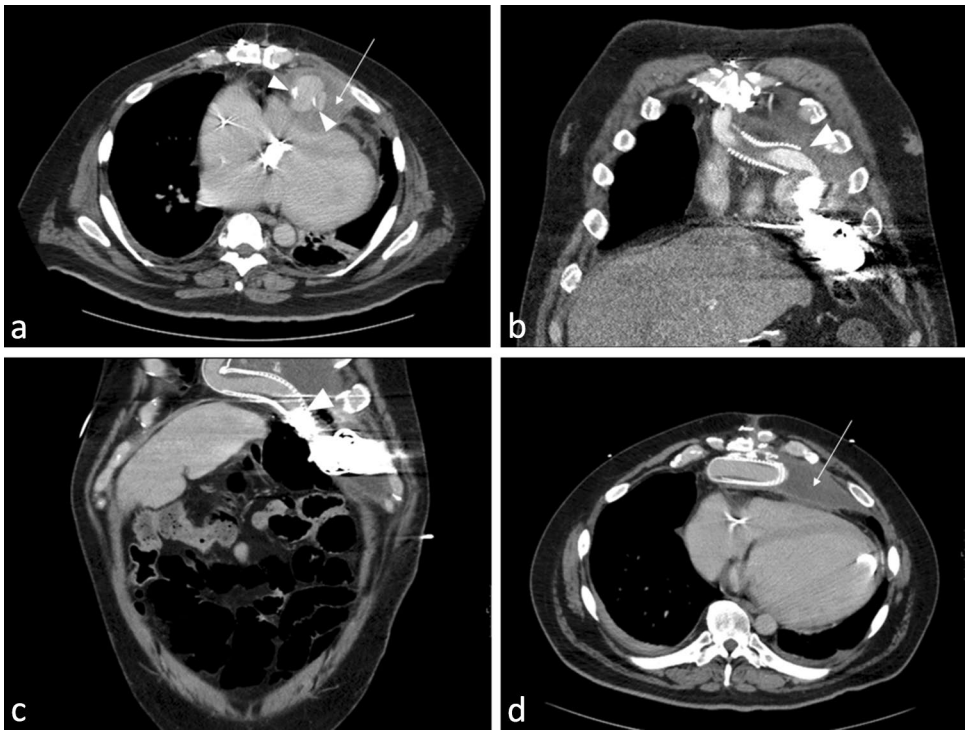

Fig. 4 44 year old male with advanced non-ischemic cardiomyopathy complicated by aortic valve disease and ventricular fibrillation status post LVAD placement. Of note, patient had laparoscopic sleeve gastrectomy that was complicated by esophageal leak. **a** Transverse image of the outflow tract. Notice the peri-anastomosis bleeding, demonstrated by contained contrast leak (arrowheads). **b** On the coronal image, there is a significant device kinking at the distal end of the device body and the proximal end of the Goretex graft (arrowhead). **c, d** Patient subsequently underwent surgical repair. Notice the original device kinking has resolved (arrowhead) on the coronal image. Transverse image again demonstrated resolving hematoma (arrow)

(^{18}F-FDG PET)/CT can be used to assess device-associated infection as well. On PET/CT, abnormally increased FDG update can be seen around the affected areas. Particularly, the inhomogeneous FDG uptake can differentiate infectious etiologies from other processes. Linear homogeneous uptake is more indicative of sterile reactive inflammation [24]. One study included 14 patients who had otherwise no external signs of infections (i.e., no driveline infection at the exit site), who presented with recurrent fever, positive blood culture, or elevated inflammatory markers. In this study PET/CT had a sensitivity of 100% and a specificity of 80% for LVAD-associated infection [25]. In addition, the FDG uptake pattern correlates with survival outcomes. Central LVAD compartment involvement is associated with higher patient mortality [26]. PET/CT scan can be used to tailor the clinical management accordingly (Figs. 5, 6, 7, 8). In the respective setting, evidence of intrathoracic component infection in CT or PET/CT may give rise to urgent listing for heart transplantation (Fig. 6).

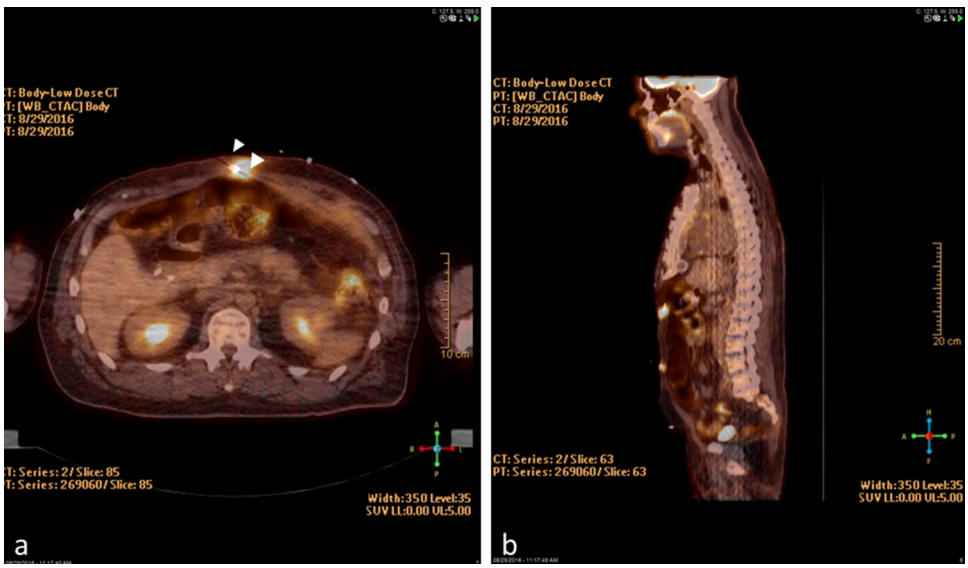

Fig. 5 Same patient subsequently developed severe driveline infection which was debrided multiple times. **a** Transverse PET/CT image shows a focus on increased FDG uptake near the skin entrance site of the driveline. Arrows mark the course of the driveline in the abdominal wall. **b** Sagittal image of the same patient. Notice again the focus of increased FDG uptake in the anterior abdominal wall, correlating with suspected driveline infection

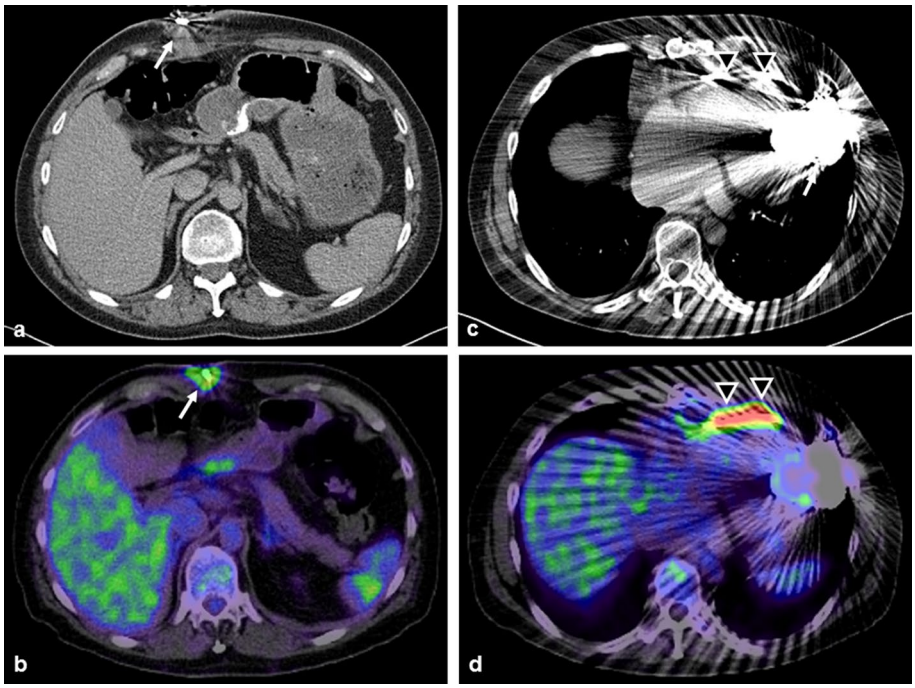

Fig. 6 54-year-old male patient with LVAD due to familial dilated cardiomyopathy. **a** CT image shows inflammatory changes tissue around the driveline (arrow) confirming the clinically suspected driveline infection. **b** The intrathoracic course of the driveline (arrow heads) is difficult to visualize on CT due to artifacts from the LVAD and the driveline itself. **c, d** FDG PET-CT was performed to evaluate intrathoracic extension of the driveline infection and revealed increased FDG uptake along both the extrathoracic (arrow) and intrathoracic courses (arrow heads) of the driveline despite the lack of systemic infection parameters. This led to a high urgency listing for heart transplantation which was successfully performed 3 months after the PET-CT. The operation confirmed the PET-CT findings

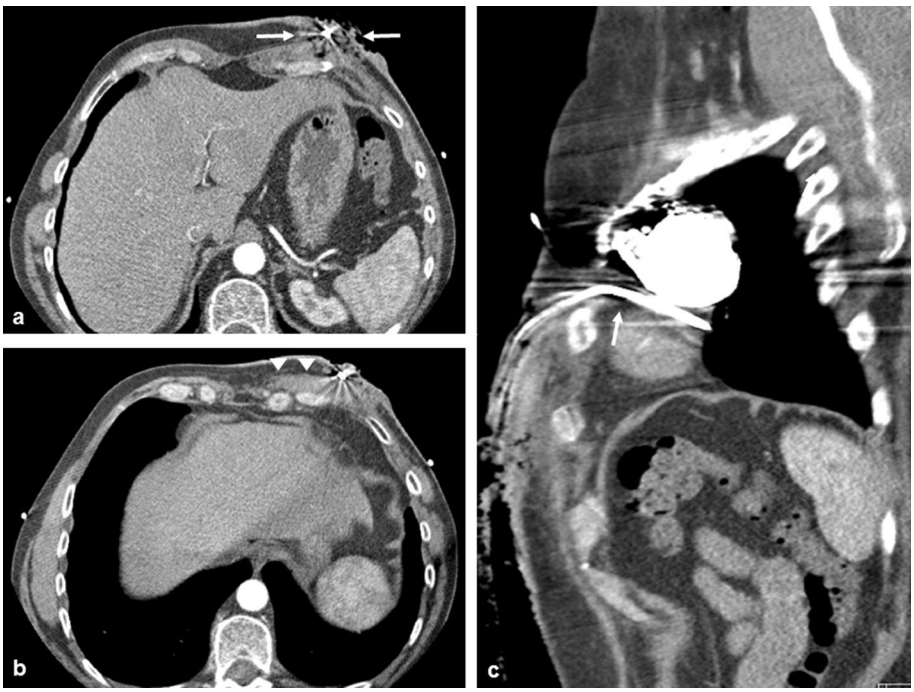

Fig. 7 47-year-old male patient with LVAD due to dilated cardiomyopathy. Negative pressure wound therapy was used due to the chronic driveline infection. **a** CT shows the infection extending along the driveline in the subcutaneous tissue down to the superficial fascia (arrow). **b** A small fluid collection can be seen medially to the driveline along the costal margin (arrow heads). **c** The fatty tissue around the intrathoracic course of the driveline deep to the anterolateral thoracotomy appears unremarkable (arrow)

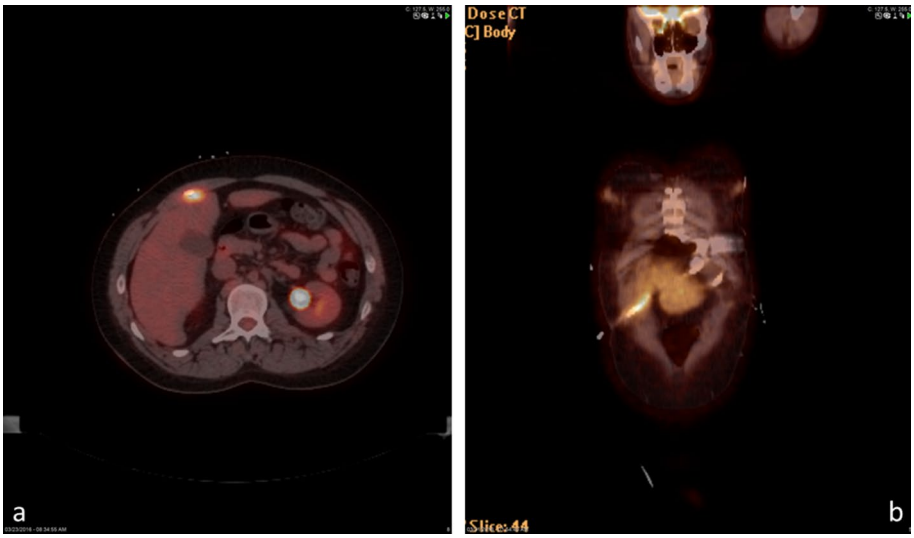

Fig. 8 Young patient with a history of non-ischemic cardiomyopathy underwent LVAD placement. Subsequently he developed chronic driveline infection. **a** Transverse image of the PET/CT shows a focus of increased FDG uptake activity in the anterior abdominal wall. **b** Corresponding coronal image again shows the increased FDG uptake tracking along the course of the driveline

Device thrombosis

Similar to the pathophysiology of device-associated infection, LVADs have blood-contacting surfaces that are biologically active with an elevated risk of inducing thrombosis. Indeed, LVAD thrombosis is a common complication in the first and second generation LVAD devices. Multiple studies reported 4–10.7% of device thrombosis in both HeartMate II and HeartWare LVADs in a pooled patient population of 559 [11, 27–29]. Device thrombosis can lead to catastrophic complications, including ischemic stroke and dramatic hemodynamic alterations. LVAD's continuous flow state increases the shear stress and activates platelets, which propagates the thrombogenic cascade [30].

It should be noted that device thrombosis is first evaluated clinically while imaging modalities can be used to definitively diagnose thrombosis. Signs of hemolysis (elevated LDH), HF (increase BNP and pro-BNP) and pump dysfunction (decreased pumping capacity at increased device power) may indicate a thrombosed device. From an imaging perspective, echocardiogram can be used to monitor issues related to device thrombosis. Outflow cannula malfunction is one of the contributing causes of LVAD thrombosis. Transthoracic echocardiogram (TTE) can evaluate cannula kinking, thrombosis, or angulation. In addition, peak flow velocity in the outflow cannula can help the diagnostic process. In a study by Grinstein et al. [31] 57 patients were evaluated for potential device thrombosis by measuring the peak flow velocity. The normal upper limit for HeartMate II was found to be 2.73 m/s and that for HeartWare HVAD was 3.42 m/s. On ultrasound exam, four patients were discovered to have outflow tract malfunction, due to either kinking or thrombosis. In those patients, the peak velocity was higher than 3.8 m/s, thereby correlating with the narrowing and obstruction of the outflow tract. A different study compared a range of echocardiographic parameters between patients with thrombosed LVAD and normal devices. Among those, there were significant differences in the diastolic flow velocity and systolic/diastolic flow velocity ratio. Outflow diastolic flow velocity was 0.7 m/s in the control group versus 0.3 m/s in the thrombosis group. Inflow and outflow systolic/diastolic velocity ratio was 1.6 and 2 versus 2.9 and 5.9 for the control group and thrombosis group, respectively in a total of 14 patients [32].

In addition, echocardiography can assess device thrombosis through a "ramp" study. Repeated echocardiography is performed at incremental pump speed. A typical protocol starts with establishing baseline characteristics at a starting pump speed of 8000 rpm. Pump speed is then increased by 400 rpm every 2 min. The left ventricular end diastolic diameter (LVEDD), pulsatile index (PI), and mitral regurgitation (MR) are measured at baseline and after each subsequent speed increase. LVEDD, PI and MR are plotted against rpm values and compared between the control and thrombosis group. A blunted or decreased LVEDD curve is highly suggestive of LVAD thrombosis [33]. Ramp study can guide early thrombolytic or anticoagulation interventions in patients presenting with signs of device thrombosis. It can also be used to assess the treatment response by following LVEDD curve slopes longitudinally during therapeutic interventions [34]. Further, the diagnostic accuracy of the ramp study can be optimized in combination with routine laboratory studies, especially in patients with underlying structural heart defects such as aortic insufficiency [35].

Apart from echocardiography, CT and catheter angiography can also be used to evaluate LVAD thrombosis. On CT imaging, thrombus is represented by low-attenuating material that creates a focal filling defect [36–39]. This is in contrast to the normal CT appearance of circumferential, hypoattenuating material with variable thickness around the

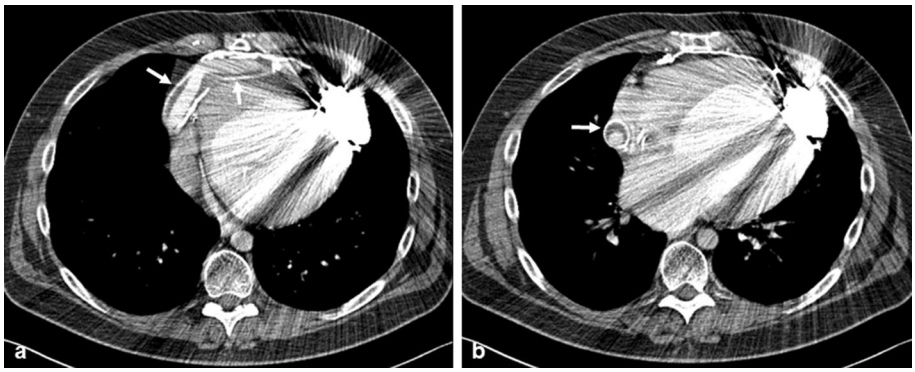

Fig. 9 41-year-old male patient with LVAD due to dilated cardiomyopathy. The Dacron graft connecting the LVAD with the ascending aorta was intraoperatively encased with a 2 mm Goretex membrane. **a, b** CT shows unremarkable perfusion of the Dacron graft and normal hypoattenuating material in the space between the Dacron graft and the Goretex membrane (arrows). This is the expected finding after such procedure. However, it could be misinterpreted as a partial thrombosis of the graft

outflow cannula (Fig. 9). On the other hand, CT is readily available to assess gross structural defects, such as inflow and outflow tract malfunction. Such defects may not be readily assessed by the echocardiography due to an inadequate acoustic window and extensive artifacts [40, 41]. Further, CT is able to evaluate the gross pathology during the entire cardiac cycle. In one case study, echocardiography revealed normal device alignment in a malfunctioned LVAD. However, on CT imaging, during systole, the inflow cannula was abutting the papillary muscle which created a temporary inflow obstruction [42].

More importantly, routine post-operative CT imaging may help guide clinical management. A recent study showed that the degree of LVAD inflow stenosis, measured by the area obstructed by either thrombus or myocardium, was positively correlated with the rate of adverse outcomes [43]. Therefore, imaging-directed medical management enables superior risk stratification. In addition, if the patient requires a subsequent pump exchange, a pre-operative CT or catheter angiography evaluation of the thrombosed LVAD can confirm mechanical etiologies and aid in presurgical planning prior to the device exchange [44] (Figs. 9, 10).

Stroke

LVAD patients are at risk both for ischemic and hemorrhagic stroke. Ischemic stroke can occur as a complication of device thrombosis. Hemorrhagic stroke can be due to the anticoagulation regimen. To complicate matters further, LVAD patients almost invariably develop acquired coagulopathies, which further increases their risk of hemorrhagic strokes [45]. The stroke rate in LVAD patients is markedly higher than that of the general population, with a reported 20-fold increased risk [46, 47]. Strokes are associated with significant morbidity and mortality in this population. Up to 18% of the LVAD patients die of a primary neurological event [7]. It is the primary cause of death in both early and late post-implantation periods [7, 48]. The mortality rate is

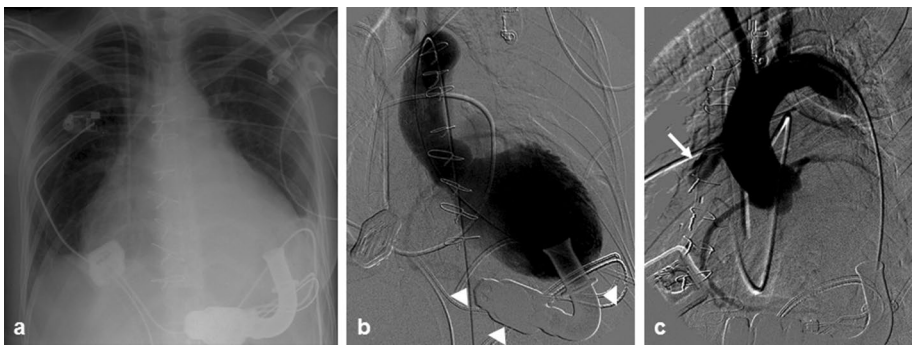

Fig. 10 60-year-old female patient with LVAD due to drug-induced cardiomyopathy. Anticoagulation was limited due to repetitive, extensive epistaxis ultimately requiring surgical treatment. **a** Chest X-ray shows the LVAD alignment. **b** Cardiac left ventriculography via transfemoral access reveals a lack of contrast flow within the cannula attached to the left ventricle and the outflow tract (arrow heads). **c** Aortography demonstrates a backflow into the outflow tract attached to the ascending aorta (arrow). These findings are suggestive of a device thrombosis which was confirmed during replacement of the device

approximately 55% for ischemic stroke, and 70% for hemorrhagic stroke at 24 months post-stroke [47]. In comparison, in the general public, the cumulative rates of all death after a stroke is 36.5 per 100,000 [49].

One contributing mechanism for the increased severity of hemorrhagic events is the acquired von Willebrand disease (vWD). In comparison to the congenital condition, acquired vWD is characterized by a qualitative change of the von Willebrand factor (vWF). In patients with LVAD, the continuous flow states creates an increased shear force in the circulatory system that disrupts the tertiary structure of vWF, which exposes its proteolytic domain to ADAMTS-13. Therefore, vWF multimer is cleaved into smaller multimers, which cannot efficiently bind to platelet surface receptors and promote primary hemostasis. As expected, LVAD patients had a decreased number of large vWF multimers [50]. This phenomenon perhaps explains the late predominance of hemorrhagic stroke and its increased mortality in comparison to the general population.

A detailed discussion of neurological imaging is beyond the scope of this review. In the LVAD population CT can be used to assess ischemic and hemorrhagic stroke. MRI is contraindicated for patients with implanted LVADs, as they contain ferromagnetic components.

Right heart failure

LVAD device implantation can induce gross physiologic shifts that precipitate functional changes. Right heart failure (RHF) is an important hemodynamic complication occurring in 20–45% of LVAD patients. Most commonly, RHF is determined by the need for right ventricular assist device insertion (after the LVAD has been implanted) and/or prolonged inotrope infusion [51–54]. RHF can result in significant morbidity and mortality. In a study by Dang et al., 42 of the 108 LVAD patients experienced right heart failure, with a higher early mortality rate (19% vs. 6.2%), and a much higher rate of re-operation and renal failure in the RHF group (38.9% vs. 18.3% and 61% vs. 22.6%, respectively) [51]. The pathophysiology of late-onset RHF is related to the underlying HF. Patients with severe HF have chronically low cardiac output, thereby leading to a decreased venous return. After LVAD implantation, there are two significant hemodynamic changes. Once an adequate cardiac output is restored, particularly in those with DT LVAD, the right ventricle sees a significant increase in venous return, which exacerbates the underlying systolic dysfunction. On the other hand, unloading of the chronically congested left ventricle causes a decrease in the left ventricular size. In turn, the ventricular septum deviates towards the left, causing a distortion of the right ventricle. The interventricular septum serves as a buttress for the right ventricular free wall contraction. In patients with right systolic dysfunction, septal contraction contributes significantly to the cardiac output as well [55]. A decrease in septal pumping may result in a further deterioration of the right cardiac output.

Right ventricular imaging is more technically challenging with echocardiography, owing to its retrosternal position, geometry and indeterminate chamber borders [56–58]. On echocardiography, RHF may present with a dilated RV, leftward shift of interventricular septum, hepatic congestion, IVC dilation, or tricuspid regurgitation. RV dilatation is often the first sign of underlying RV dysfunction. Although echocardiography is the most widely used, retrospectively ECG-gated CT can also be used to assess the right ventricular anatomy and function. Studies in non LVAD patients have shown good correlation between CT and cardiac MRI, although RV ejection fraction measurement correlated only moderately ($r = 0.86$) [59].

Imaging techniques can help predict and evaluate RHF after LVAD implantation. Echocardiography is the most commonly used modality. Echocardiographic parameters measure right ventricular volume and wall motion abnormalities, thereby estimating the systolic function. One of the parameters is the tricuspid annular plane systolic excursion (TAPSE), measuring the two-dimensional lateral tricuspid annular movement [60–62]. In a normal patient, the annulus moves towards the apex during systole. Therefore, a smaller value is indicative of worse systolic function [63, 64]. Another predictor of RHF is the RV/LV diameter ratio, which can be used as a marker for right ventricular remodeling and strain. A value < 0.75 has demonstrated an independent association with RHF in continuous-flow LVAD [65]. Multiple studies have shown that pre-operative tricuspid valve incompetence was more severe in the group developed RHF compared to the non-RHF group in LVAD patients [66, 67]. In addition, the absolute value of RV longitudinal strain obtained from speckle tracking echocardiography was lower in the patient group with RHF in comparison to the group without [68].

Gastrointestinal bleeding

Another important complication post LVAD device implantation includes gastrointestinal bleeding (GIB), affecting approximately 18.6–22.8% of patients [69–72]. Further, LVAD patients have more severe bleeding episodes, often necessitating transfusion of 2–8 units of packed red blood cells [69]. Multiple transfusions can lead to the development of antibodies against circulating blood products and tissue antigens, thereby making future heart transplantation challenging. There is evidence showing that the continuous flow state is a direct risk factor for GIB. One large retrospective review has shown a 3.24-fold increase in GIB risk associated with continuous-flow LVADs in comparison to pulsatile LVADs [73]. More interestingly, increased systolic

pulsatility was associated with a lower incidence of GIB in continuous-flow LVADs [74], thereby reaffirming the role of the pulseless state in inducing GIB.

GIB can certainly manifest through a mechanism similar to that of LVAD-associated hemorrhagic stroke, namely, the anticoagulation regimen and the acquired vWD. However, LVAD-associated GIB is also related to the formation of angiodysplasia. LVAD patients often develop angiodysplasia in the upper GI tract and small bowel while the age-related angiodysplasia in the elderly typically occurs in the right colon where the wall stress is the highest [75]. One theory proposed the pathophysiology may be related to a decreased end-organ perfusion with a non-pulsatile state, even though the mean arterial pressure is adequate [76]. Therefore, the resulting local hypoxia promotes angiogenesis.

From an imaging perspective, a wide range of imaging modalities can be used to assess the occult GIB, including tagged red blood cell scanning, CTA and catheter-directed angiography. Radionuclide scanning with technetium labelled red blood cells can localize slow-flowing bleeding source at a speed as low as 0.04 mL/min in animal models [77]. This imaging modality has a 93% sensitivity and 95% specificity for any bleeding within the GI tract [78]. The localization accuracy ranges from 86 to 91% [79–81]. In comparison, CTA can also produce an accurate depiction of the actively bleeding vessel and enables detection of arteriovenous malformations during the arterial phase [82]. CTA can complement endoscopy in diagnosing GIB which typically appears as a spot of intraluminal contrast in the arterial phase enlarging in the venous and late phases. It may also identify the supplying artery. The pooled diagnostic yield of CTA is 40% versus 53% for endoscopy [83]. Invasive angiography is reserved for accurate localization and transcatheter embolization to treat the bleeding source.

Aortic hemodynamic changes

Another important hemodynamic change post LVAD device implantation relates to the gross physiological adaptations with respect to blood flow redistribution. Computational models have shown that the placement of the outflow cannula can influence the local blood flow pattern. A study by Kar et al. showed that when the outflow cannula was positioned in the descending aorta, a region of stagnant flow was appreciated in the backflow portion. Furthermore, at increased LVAD output, the native aortic valve remained closed throughout the cycle leading to stagnant flow at the aortic root. Such stagnation zones may cause the formation of thrombosis and ultimately embolic events. In comparison, the ascending aortic anastomosis approach was superior in terms of reducing the stagnation zone even though the zone still persisted [84]. In another study, two patients were scanned with CT angiography to obtain a detailed anatomical depiction of the aorta and the outflow cannula. In one patient, the outflow cannula anastomosed with the ascending aorta in the anterior aspect while the other was anastomosed in the lateral aspect. Computational fluid dynamics (CFD) were constructed and echocardiography was used to obtain the physiological data for the simulation. Streamlines, dynamic wall pressure and quantitative hemodynamics were obtained from the imaging model. In the patient with the anterior anastomosis, there was a focal spot of high dynamic pressure exceeding 900 Pa. In addition, wall stress, total pressure and velocity magnitude were significantly higher in the patient with anterior anastomosis [85]. Another CFD study enrolled five patients. CT angiography was performed to assess the geometry of the cannula and aorta. Further, the anatomical relationship between the graft and the native aorta was characterized by the lateral and horizontal angles. For example, the polar angle was defined as the angle between the midlines of the outflow cannula and ascending aorta. The azimuth angle was defined as the angle between the midline of the outflow cannula and the line between the midpoints of ascending and descending aorta. CFD model was constructed based on the Navier–Stokes equations and streamlines, wall stress and turbulence models were generated. The simulation results showed that with increasing angles, there was an associated increase in wall stress and turbulence. These alterations in hemodynamics may lead to a zone of stasis and thrombosis in the aorta. Further, the shear stress can lead to structural remodeling since it causes activation of matrix metalloproteinases. Valvular leaflets remodeling can lead to further hemodynamic complications, namely aortic insufficiency [86]. Further CFD studies discovered that the pulsatile LVAD may have a more benign hemodynamics pattern compared to the continuous-flow LVADs with regard to wall stress and turbulence. The average retrograde dynamic pressure was 0.14 mmHg in the continuous group versus 0.013 mmHg in the pulsatile group [87]. Based on these results, resumption of periodic pulsatility may be beneficial in LVAD patients.

Conclusion

LVAD was born out of necessity due to a shortage of available donor hearts. Over the past four decades, the evolution of LVAD has led to smaller, more compact designs that are increasingly biocompatible. Early clinical trials have shown a significant survival benefit of LVAD in comparison to medical management alone. However, adverse event rate remains high. Bleeding, thrombosis, infection, embolic events, and hemodynamic changes are among the most common complications. As LVAD is becoming increasingly utilized, radiologists should be familiar with the imaging features of associated complications. Multiple imaging

modalities can be used to assess the LVAD complications, particularly CTA, echocardiography, PET-CT and catheter angiography. CTA is particularly useful in assessing bleeding complications and device thrombosis. Echocardiography is particularly useful in assessing right heart failure post LVAD implantation. Lastly, PET-CT has unique utility in assessing device-related infections.

Author contributions XL participated in the concept creation, literature search, review, drafting, VK participated in the drafting and editing, ST participated in the drafting, editing and concept creation, AR participated in the drafting, SA participated in the concept creation and editing, AD participated in the concept creation and editing, SP participated in the concept creation, drafting, literature review and editing, FR participated in the drafting and editing.

Compliance with ethical standards

Conflict of interest All authors declare that they have no conflict of interest.

References

1. Roger VL et al (2011) Heart disease and stroke statistics-2011 update: a report from the American Heart Association. Circulation 123(4):e18–e209
2. Roger VL (2013) Epidemiology of heart failure. Circ Res 113(6):646–659
3. Rose EA et al (2001) Long-term use of a left ventricular assist device for end-stage heart failure. N Engl J Med 345(20):1435–1443
4. Burnett H et al (2017) Thirty years of evidence on the efficacy of drug treatments for chronic heart failure with reduced ejection fraction: a network meta-analysis. Circ Heart Fail 10(1):e003529
5. Yancy C et al (2013) 2013 ACCF/AHA guideline for the management of heart failure: a report of the American college of cardiology foundation/american heart association task force on practice guidelines. J Am Coll Cardiol 62(16):1495–1539
6. Kirklin JK et al (2017) Eighth annual INTERMACS report: Special focus on framing the impact of adverse events. J Heart Lung Transplant 36(10):1080–1086
7. Kirklin JK et al (2015) Seventh INTERMACS annual report: 15,000 patients and counting. J Heart Lung Transplant 34(12):1495–1504
8. Sandner SE et al (2009) Age and outcome after continuous-flow left ventricular assist device implantation as bridge to transplantation. J Heart Lung Transpl 28(4):367–372
9. Mi E, DeBakey (1997) Development of a ventricular assist device. Artif Organs 21(11):1149–1153
10. Lietz K et al (2007) Outcomes of left ventricular assist device implantation as destination therapy in the post-REMATCH era. Circulation 116(5):497–505
11. Slaughter MS et al (2009) Advanced heart failure treated with continuous-flow left ventricular assist device. N Engl J Med 361(23):2241–2251
12. Heatley G et al (2016) Clinical trial design and rationale of the multicenter study of MagLev Technology in patients undergoing mechanical circulatory support therapy with heartmate 3 (MOMENTUM 3) investigational device exemption clinical study protocol. J Heart Lung Transpl 35(4):528–536
13. Pinney SP, Anyanwu AC, Lala A, Teuteberg JJ, Uriel N, Mehra MR (2017) Left ventricular assist devices for lifelong support. J Am Coll Cardiol 69(23):2845–2861
14. Starling RC et al (2017) Risk assessment and comparative effectiveness of left ventricular assist device and medical management in ambulatory heart failure patients: the ROADMAP study 2-year results. JACC Heart Fail 5(7):518–527
15. Carr CM, Jacob J, Park SJ, Karon BL, Williamson EE, Araoz PA (2010) CT of left ventricular assist devices. RadioGraphics 30(2):429–444
16. Huang CH, Liu CL, Chen WK (2009) Periportal edema and ascites: computed tomographic signs of traumatic cardiac tamponade. Am J Emerg Med 27(1):e3–127
17. Hernández-Luyando L, Calvo J, González E, De L Heras, De La Puente H, López C (1996) Tension pericardial collections: sign of 'flattened heart' in CT. Eur J Radiol 23(3):250–252
18. Frazier OH et al (2001) Research and development of an implantable, axial-flow left ventricular assist device: the Jarvik 2000 Heart. in Ann Thorac Surg 71(3 Suppl):S125–S132
19. Sharma V et al (2012) Driveline infections in left ventricular assist devices: implications for destination therapy. Ann Thorac Surg 94(5):1381–1386
20. Yarboro LT et al (2014) Technique for minimizing and treating driveline infections keynote lecture series. Ann Cardiothorac Surg 3(6):557–562
21. Zierer A et al (2007) Late-onset driveline infections: the achilles' heel of prolonged left ventricular assist device support. Ann Thorac Surg 84(2):515–520
22. Chaparro S, Hernandez G, Breton JN (2017) Driveline infection in ventricular assist devices and its implication in the present era of destination therapy. Open J Cardiovasc Surg 9:1179065217714216
23. Topkara VK et al (2010) Infectious complications in patients with left ventricular assist device: etiology and outcomes in the continuous-flow era. Ann Thorac Surg 90(4):1270–1277
24. Spacek M, Belohlavek O, Votrubova J, Sebesta P, Stadler P (2009) Diagnostics of "non-acute" vascular prosthesis infection using 18F-FDG PET/CT: our experience with 96 prostheses. Eur J Nucl Med Mol Imaging 36(5):850–858
25. Dell'Aquila AM et al (2016) Contributory role of Fluorine 18-fluorodeoxyglucose positron emission Tomography/Computed tomography in the diagnosis and clinical management of infections in patients supported with a continuous-flow left ventricular assist device. Ann Thorac Surg 101(1):87–94
26. Kim J, Feller ED, Chen W, Liang Y, Dilsizian V (2018) FDG PET/CT for early detection and localization of left ventricular assist device infection. Impact on patient management and outcome. JACC: Cardiovasc Imaging. https://doi.org/10.1016/j.jcmg.2018.01.024
27. Najjar SS et al (2014) An analysis of pump thrombus events in patients in the HeartWare ADVANCE bridge to transplant and continued access protocol trial. J Heart Lung Transpl 33(1):23–34
28. Uriel N et al (2014) Device thrombosis in HeartMate II continuous-flow left ventricular assist devices: a multifactorial phenomenon. J Heart Lung Transpl 33(1):51–59
29. Slaughter MS (2010) Hematologic effects of continuous flow left ventricular assist devices. J Cardiovasc Transl Res 3(6):618–624
30. Tamari Y et al (1975) Functional changes in platelets during extracorporeal circulation. Ann Thorac Surg 19(6):639–647
31. Grinstein J et al (2016) Screening for outflow cannula malfunction of left ventricular assist devices (LVADs) with the use of doppler echocardiography: new LVAD-specific reference values for contemporary devices. J Card Fail 22(10):808–814
32. Fine NM et al (2013) Role of echocardiography in patients with intravascular hemolysis due to suspected continuous-flow LVAD thrombosis. JACC Cardiovasc Imaging 6(11):1129–1140

33. Uriel N et al (2012) Development of a novel echocardiography ramp test for speed optimization and diagnosis of device thrombosis in continuous-flow left ventricular assist devices: the Columbia ramp study. J Am Coll Cardiol 60(18):1764–1775
34. Kato TS et al (2014) Value of serial echo-guided ramp studies in a patient with suspicion of device thrombosis after left ventricular assist device implantation. Echocardiography 31(1):E5–E9
35. Adatya S et al (2015) Echocardiographic ramp test for continuous-flow left ventricular assist devices. JACC Heart Fail 3(4):291–299
36. Lazoura O et al (2016) A low-dose, dual-phase cardiovascular CT protocol to assess left atrial appendage anatomy and exclude thrombus prior to left atrial intervention. Int J Cardiovasc Imaging 32(2):347–354
37. Teunissen C, Habets J, Velthuis BK, Cramer MJ, Loh P (2017) Double-contrast, single-phase computed tomography angiography for ruling out left atrial appendage thrombus prior to atrial fibrillation ablation. Int J Cardiovasc Imaging 33(1):121–128
38. Tatli S, Lipton MJ (2005) CT for intracardiac thrombi and tumors. Int J Cardiovasc Imaging 21:115–131
39. Mishkin JD et al (2012) Utilization of cardiac computed tomography angiography for the diagnosis of left ventricular assist device thrombosis. Circ Heart Fail 5(2):e27–e29
40. Chrysant GS, Phancao AA, Horstmanshof DA, Jones S, Long JW (2018) Clinical utility of imaging left ventricular assist devices with 320 row multidetector computed tomography. ASAIO J 64(6):760–765
41. Obi CA, Chan N, Rizkalla MG, Makaryus JN (2018) Assessment of cardiac thrombosis in patients with left ventricular assist device using multidetector cardiac computed tomography. J Cardiovasc Med 19(7):389–390
42. Acharya D et al (2013) use of retrospectively gated CT angiography to diagnose systolic LVAD inflow obstruction. ASAIO J 59(5):542–546
43. Sacks J et al (2015) Utility of cardiac computed tomography for inflow cannula patency assessment and prediction of clinical outcome in patients with the HeartMate II left ventricular assist device. Interact Cardiovasc Thorac Surg 21(5):590–593
44. Yu SN et al (2018) Role of computed tomography angiography for HeartMate II left ventricular assist device thrombosis. Int J Artif Organs 41(6):325–332
45. Muslem R, Caliskan K, Leebeek FWG (2018) Acquired coagulopathy in patients with left ventricular assist devices. J Thromb Haemost 16(3):429–440
46. Mozaffarian D et al (2016) Executive summary: heart disease and stroke statistics-2016 update: a report from the American Heart Association. Circulation 133(4):447–454
47. Acharya D et al (2017) INTERMACS analysis of stroke during support with continuous-flow left ventricular assist devices: risk factors and outcomes. JACC Heart Fail 5(10):703–711
48. Kirklin JK et al (2014) Sixth INTERMACS annual report: a 10,000-patient database. J Heart Lung Transpl 33(6):555–564
49. Benjamin EJ, Blaha MJ, Chiuve SE, Cushman M (2017) Heart disease and stroke statistics—2017 update. Circulation 135(10):e146–e603
50. Uriel N et al (2010) Acquired von Willebrand syndrome after continuous-flow mechanical device support contributes to a high prevalence of bleeding during long-term support and at the time of transplantation. J Am Coll Cardiol 56(15):1207–1213
51. Dang NC et al (2006) Right heart failure after left ventricular assist device implantation in patients with chronic congestive heart failure. J Heart Lung Transpl 25(1):1–6
52. Kormos RL et al (2010) Right ventricular failure in patients with the HeartMate II continuous-flow left ventricular assist device: incidence, risk factors, and effect on outcomes. J Thorac Cardiovasc Surg 139(5):1316–1324
53. Kapelios CJ et al (2015) Late-onset right ventricular dysfunction after mechanical support by a continuous-flow left ventricular assist device. J Heart Lung Transpl 34(12):1604–1610
54. Kavarana MN et al (2002) Right ventricular dysfunction and organ failure in left ventricular assist device recipients: a continuing problem. Ann Thorac Surg 73(3):745–750
55. Weber KT, Janicki JS, Shroff S, Fishman AP (1981) Contractile mechanics and interaction of the right and left ventricles. Am J Cardiol 47(3):686–695
56. Morcos P, Vick GW, Sahn DJ, Jerosch-Herold M, Shurman A, Sheehan FH (2009) Correlation of right ventricular ejection fraction and tricuspid annular plane systolic excursion in tetralogy of fallot by magnetic resonance imaging. Int J Cardiovasc Imaging 25(3):263–270
57. Tamborini G et al (2018) Multi-parametric 'on board' evaluation of right ventricular function using three-dimensional echocardiography: feasibility and comparison to traditional two-and three dimensional echocardiographic measurements. Int J Cardiovasc Imaging. https://doi.org/10.1007/s10554-018-1496-9
58. Driessen MMP et al (2014) Pressure overloaded right ventricles: a multicenter study on the importance of trabeculae in RV function measured by CMR. Int J Cardiovasc Imaging 30(3):599–608
59. Raman SV, Shah M, McCarthy B, Garcia A, Ferketich AK (2006) Multi-detector row cardiac computed tomography accurately quantifies right and left ventricular size and function compared with cardiac magnetic resonance. Am Heart J 151(3):736–744
60. Korshin A et al (2018) The feasibility of tricuspid annular plane systolic excursion performed by transesophageal echocardiography throughout heart surgery and its interchangeability with transthoracic echocardiography. Int J Cardiovasc Imaging 34(7):1017–1028
61. Forner AF, Hasheminejad E, Sabate S, Ackermann MA, Turton EW, Ender J (2017) Agreement of tricuspid annular systolic excursion measurement between transthoracic and transesophageal echocardiography in the perioperative setting. Int J Cardiovasc Imaging 33(9):1385–1394
62. Schneider M et al (2018) Echocardiographic assessment of right ventricular function: current clinical practice. Int J Cardiovasc Imaging 35(1):49–56
63. Puwanant S et al (2008) Tricuspid annular motion as a predictor of severe right ventricular failure after left ventricular assist device implantation. J Heart Lung Transpl 27(10):1102–1107
64. Sato T et al (2013) Simple prediction of right ventricular ejection fraction using tricuspid annular plane systolic excursion in pulmonary hypertension. Int J Cardiovasc Imaging 29(8):1799–1805
65. Vivo RP et al (2013) Increased right-to-left ventricle diameter ratio is a strong predictor of right ventricular failure after left ventricular assist device. J Heart Lung Transpl 32(8):792–799
66. Potapov EV et al (2008) Tricuspid incompetence and geometry of the right ventricle as predictors of right ventricular function after implantation of a left ventricular assist device. J Heart Lung Transpl 27(12):1275–1281
67. Baumwol J et al (2011) Right heart failure and 'failure to thrive' after left ventricular assist device: clinical predictors and outcomes. J Heart Lung Transpl 30(8):888–895
68. Kato TS et al (2013) Serial Echocardiography using tissue doppler and speckle tracking imaging to monitor right ventricular failure before and after left ventricular assist device surgery. JACC Heart Fail 1(3):216–222
69. Demirozu ZT et al (2011) Arteriovenous malformation and gastrointestinal bleeding in patients with the HeartMate II left ventricular assist device. J Heart Lung Transpl 30(8):849–853
70. Aggarwal A et al (2012) Incidence and management of gastrointestinal bleeding with continuous flow assist devices. Ann Thorac Surg 93(5):1534–1540

71. Morgan J et al (2012) Gastrointestinal bleeding with the HeartMate II left ventricular assist device. J Heart Lung Transpl 31(7):715–718
72. Kushnir VM et al (2012) Evaluation of GI bleeding after implantation of left ventricular assist device. Gastrointest Endosc 75(5):973–979
73. Joy PS, Kumar G, Guddati AK, Bhama JK, Cadaret LM (2016) Risk factors and outcomes of gastrointestinal bleeding in left ventricular assist device recipients. Am J Cardiol 117:240–244
74. Wever-Pinzon O et al (2013) Pulsatility and the risk of nonsurgical bleeding in patients supported with the continuous-flow left ventricular assist device heartmate II. Circ Heart Fail 6(3):517–526
75. Marsano J, Desai J, Chang S, Chau M, Pochapin M, Gurvits GE (2015) Characteristics of gastrointestinal bleeding after placement of continuous-flow left ventricular assist device: a case series. Dig Dis Sci 60(6):1859–1867
76. Cappell MS, Lebwohl O (1986) Cessation of recurrent bleeding from gastrointestinal angiodysplasias after aortic valve replacement. Ann Intern Med 105(1):54–57
77. Thorne DA, Datz FL, Remley K, Christian PE (1987) Bleeding rates necessary for detecting acute gastrointestinal bleeding with technetium-99m-labeled red blood cells in an experimental model. J Nucl Med 28(4):514–520
78. Bunker SR et al (1984) Scintigraphy of gastrointestinal hemorrhage: superiority of 99mTc red blood cells over 99mTc sulfur colloid. Am J Roentgenol 143(3):543–548
79. Dusold R, Burke K, Carpentier W, Dyck WP (1994) The accuracy of technetium-99m-labeled red cell scintigraphy in localizing gastrointestinal bleeding. Am J Gastroenterol 89(3):345–348
80. Markisz JA, Front D, Royal HD, Sacks B, Parker JA, Kolodny GM (1982) An evaluation of 99mTc-labeled red blood cell scintigraphy for the detection and localization of gastrointestinal bleeding sites. Gastroenterology 83(2):394–398
81. Emslie JT, Zarnegar K, Siegel ME, Beart RW (1996) Technetium-99m-labeled red blood cell scans in the investigation of gastrointestinal bleeding. Dis Colon Rectum 39(7):750–754
82. Huprich jamesE, Barlow JM, Hansel SL, Alexander JA, Fidler JL (2013) Multiphase CT enterography evaluation of small-bowel vascular lesions. AJR 201:65–72
83. Wang Z, Chen J, Liu J, Qin X, Huang Y (2013) CT enterography in obscure gastrointestinal bleeding: a systematic review and meta-analysis. J Med Imaging Radiat Oncol 57(3):263–273
84. Kar B et al (2005) The effect of LVAD aortic outflow-graft placement on hemodynamics and flow: implantation technique and computer flow modeling. Tex Heart Inst J 32(3):294–298
85. Karmonik C et al (2012) Influence of LVAD cannula outflow tract location on hemodynamics in the ascending aorta: a patient-specific computational fluid dynamics approach. ASAIO J 58(6):562–567
86. Karmonik C et al (2014) computational fluid dynamics in patients with continuous-flow left ventricular assist device support show hemodynamic alterations in the ascending aorta. J Thorac Cardiovasc Surg 147(4):1326–1333
87. Karmonik C et al (2014) Comparison of hemodynamics in the ascending aorta between pulsatile and continuous flow left ventricular assist devices using computational fluid dynamics based on computed tomography images. Artif Organs 38(2):142–148